# Holographically fabricated, highly reflective nanoporous polymeric distributed Bragg reflectors with red, green, and blue colors [Invited]

**Haodong Jiang (蒋皓东)[1,2], Wenfeng Cai (蔡文锋)[1], Ke Li (李 珂)[1,3], Ming Cheng (成 茗)[1], Vineet Kumar[1], Zhen Yin (殷 震)[1], Davy Gérard[3], Dan Luo (罗 丹)[1], Quanquan Mu (穆全全)[4], and Yanjun Liu (刘言军)[1,4,5,*]**

[1]*Department of Electrical and Electronic Engineering, Southern University of Science and Technology, Shenzhen 518055, China*

[2]*Harbin Institute of Technology, Harbin 150001, China*

[3]*Light, Nanomaterials, Nanotechnologies (L2n), Université de Technologie de Troyes & CNRS ERL 7004, Troyes 10004, France*

[4]*State Key Laboratory of Applied Optics, Changchun Institute of Optics, Fine Mechanics and Physics, Chinese Academy of Sciences, Changchun 130033, China*

[5]*Key Laboratory of Energy Conversion and Storage Technologies (Southern University of Science and Technology), Ministry of Education, Shenzhen 518055, China*

**Corresponding author: yjliu@sustech.edu.cn*

Received June 25, 2020; accepted July 7, 2020; posted online July 21, 2020

We report holographic fabrication of nanoporous distributed Bragg reflector (DBR) films with periodic nanoscale porosity via a single-prism conuration. The nanoporous DBR films result from the phase separation in a material recipe, which consists of a polymerizable acrylate monomer and nonreactive volatile solvent. By changing the interfering angle of two laser beams, we achieve the nanoporous DBR films with highly reflective red, green, and blue colors. The reflection band of the nanoporous DBR films can be tuned by further filling different liquids into the pores inside the films, resulting in the color change accordingly. Experimental results show that such kinds of nanoporous DBR films could be potentially useful for many applications, such as color filters and refractive index sensors.

*Keywords: distributed Bragg reflector; nanoporous reflection grating; holographic fabrication; phase separation; refractive index sensing.*

*doi: 10.3788/COL202018.080007.*

A distributed Bragg reflector (DBR)[1] is a periodic structure formed from alternating dielectric layers that can be used to achieve near unit reflectance within a range of frequencies. By designing DBR films with different periods and refractive indices, one can selectively achieve reflection or transmission of specific wavelengths of light[2]. In the past decades, DBR films have been widely used in sensors[3], displays[4], lasers[5], LEDs[6], and other optoelectronic devices[7,8]. Thus far, DBR films are typically fabricated via evaporation and coating techniques, such as physical/chemical deposition, spin-coating, and Langmuir–Blodgett coating. However, these techniques usually require complicated multi-step processes, long fabrication time, or costly facilities, hence limiting further development of DBR applications. Therefore, it is highly desired to develop a simple, fast, and cost-effective technique to fabricate the DBR films.

Along this line, the laser holographic technique could be the best option since it provides a single-step and rapid fabrication process for highly ordered structures. A typical holographic process starts with a photopolymerizable prepolymer material. Upon holographic exposure, the cured photopolymer gives rise to periodic index modulations that are governed by the interference pattern of coherent laser beams[9,10]. Depending on the interference configurations, one-, two-, or three-dimensional (1D, 2D, or 3D) periodic structures can be created. By adding the nonreactive liquid crystals (LCs) into the prepolymer mixture, one can therefore achieve the ordered polymer-LC structures with tunable optical properties, resulting in many useful photonic applications[11–19]. This LC-involving patterning process is widely known as the holographic polymer-dispersed LC (HPDLC) technique[20,21]. Similarly, the addition of other additives such as nanoparticles into these holographic formulations has been also investigated[22–24]. Simultaneous addition of LCs and nanoparticles in the HPDLC formulation is expected to achieve the ordered structures with enhanced optical properties[25–27].

The 1D HPDLC periodic structures (i.e., gratings) are natural DBRs[28–34], which have been extensively investigated for many applications[35–38]. Particularly, the 1D HPDLC reflection gratings have long been studied for optical filters and reflective displays[32]. For the grating fabrication, the nature of coherent light illumination and the viscosity of the prepolymer syrup affect the phase separation of LC and polymer significantly during the

 

photopolymerization process. Usually, upon the LCs partially separate from the polymer, numerous optically anisotropic LC droplets are formed, which will further cause nonnegligible light scattering. As a result, strong light scattering could kill the phase separation due to polymerization in a patterned periodic fashion[39–41], leading to formation of a poor-quality grating. This effect can be greatly suppressed by elevating the polymerization temperature above the clearing point of LCs. The elevated temperature decreases not only the anisotropy effect of LCs, but also the viscosity of the prepolymer syrup that greatly facilitates the phase separation[39,40]. Another possible way is to add the nonreactive additive. Hsiao and coworkers have reported porous reflection gratings fabricated from an acetone-added HPDLC formulation using visible (Vis) laser (wavelength: 514 nm) holography[42–44]. Applications including humidity sensors have been also demonstrated[45–47]. However, only red-color reflection gratings can be achieved at the normal incidence using the Vis laser holography technique. In addition, the reflectance of nanoporous DBRs is still not high enough, and the reflection band is a bit wide due to the strong scattering, which greatly limits their further applications.

In this work, we report highly reflective nanoporous DBRs with a modified HPDLC formulation via a single-prism-based ultraviolet (UV) interference setup. By changing the interference angle, nanoporous DBRs with three primary colors (red, green, and blue) are achieved after the removal of LCs. Such a kind of nanoporous DBR is potentially useful for various applications including sensors, filters, holograms, etc.

In our experiments, the prepolymer syrup consists of 30 wt% nematic LC E7 (Jiangsu Hecheng Display Co., Ltd.), 40 wt% reactive mixture, and 30 wt% volatile solvent, acetone (Shanghai Lingfeng Chemical Reagent Co., Ltd.). The reactive mixture consists of 35 wt% monomer, trimethylolpropane triacrylate (TMPTA, Aldrich), 3 wt% cross-linking monomer, RM257 (Shijiazhuang Stiano Fine Chemical Co., Ltd.), 1 wt% UV photoinitiator 1173 (2-hydroxy-2-methylpropiophenone, Aldrich), 1 wt% co-initiator, and N-phenylglycine (NPG, Aldrich).

All of the materials were homogeneously mixed at 45°C by stirring at 1000 rad/s for 2 h. Then, we added acetone into the mixture. An LC cell was assembled with two pieces of cleaned soda glass (size: 4 cm × 2 cm) using the optical adhesive NOA65. The cell gap was controlled to be 10 μm using the $SiO_2$ ball spacers. The prepolymer syrup was then injected into the LC cell via the capillary action.

The reflection spectra of nanoporous DBR films were measured using a UV–Vis–near-infrared (NIR) microspectrophotometer (CRAIC 20/30 PV™) with a 75 W broadband xenon light source. The probe light beam was focused to have a detecting area of 15 μm × 15 μm using a 36× objective lens combined with a variable aperture. The morphologies of nanoporous DBR films were investigated by field emission scanning electron microscopy (FESEM, Merlin, Zeiss) at an acceleration voltage of 5 kV. For the refractive index sensing test, four solvents with

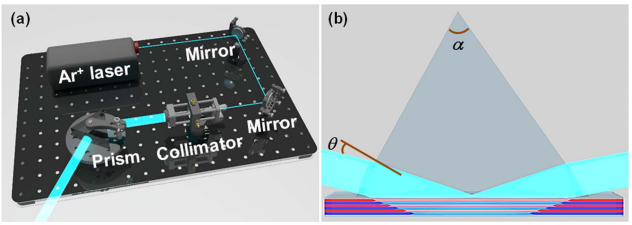


Fig. 1. (a) Experimental setup for fabricating DBR films. (b) Schematic optical interference inside the LC cell via the single-prism configuration.

different refractive indices were used. They were methanol ($n_m = 1.328$), ethanol ($n_e = 1.361$), *n*-propanol ($n_p = 1.384$), and *n*-butanol ($n_b = 1.399$), respectively.

The experimental setup of the single-prism-based holography system is schematically illustrated in Fig. 1(a). An $Ar^+$ laser (model: Innova 306C, wavelength: 363.6 nm, Coherent, USA) was used as the light source. The output laser beam was subsequently filtered, expanded, and then collimated with a beam size of 2 cm in diameter. The collimated laser beam was then impinged on a designed prism. At a certain incident angle, total internal reflection took place for the incident laser beam at the glass–air interface of the prism. As a result, the incident beam and its own total internally reflected beam interfered with each other and formed a periodic interference pattern. The designed prism is made of quartz and has an apex angle of $\alpha = 64°$ with the purpose of achieving red-color nanoporous DBR films and having the ease of adjusting the incident angle as well. An LC cell filled with the prepolymer syrup was in optical contact with the base of the prism using an index-matching oil to further form the interference pattern inside the cell. Figure 1(b) shows the specific optical path of the laser in the prism and LC cell. With the help of the matching oil, the laser beam entered the LC cell and was totally reflected at the glass–air interface. The prism was placed on a rotation stage for the ease of changing the incident angle $\theta$ of the collimated laser beam. By doing so, the period of the interference pattern can be conveniently changed. As a result, we can achieve the polymeric DBR films with different periods. All the experiments were carried out at room temperature.

To estimate the period of the interference pattern, we have carried out the simulation of the laser interference based on the prism using the finite-difference time-domain (FDTD) method. The wavelength of a monochromatic light source was set to be 364 nm. The refractive index of the prism is 1.47. In our simulation, we have set three different incident angles of 7°, 14°, and 21°, respectively. The simulation results are shown in Fig. 2. It is obvious

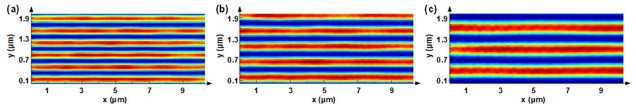


Fig. 2. Simulated interference patterns with three different incident angles of (a) 7°, (b) 14°, and (c) 21°, respectively.

that the period of the interference pattern becomes large as the incident angle increases. The simulated periods at the three incident angles were ~350 nm, ~450 nm, and ~650 nm, respectively. From the simulation results, we can therefore carry out the experiments for the fabrication of DBR films.

Upon exposure to the interference patterning with the beam intensity of 10 mW/cm$^2$ for 2 min, the LC cells were then exposed to UV light for ~30 min with the exposure intensity of 10 mW/cm$^2$ and then post-cured for 24 h in air to ensure complete polymerization. Upon opening the LC cell to separate the cured sample from one cover slide, the acetone inside the cured sample will evaporate rapidly, and a nanoporous polymeric DBR film situated on the other cover slide was then achieved. It is worth mentioning that when the cell was opened, the DBR films tended to situate on the cover slide that was nearest to the incoming light. We noticed that there was a big difference on the appearance of the sample before and after the cell opening. The sealed LC cells after the UV laser exposure demonstrate a totally transparent state, as shown in Figs. 3(a1) and 3(a2). The total transparency can be mainly attributed to the index matching due to the presence of an isotropic solvent (i.e., acetone). However, the nanoporous polymeric DBR film presents a translucent state [see Figs. 3(b1) and 3(b2)]. The evaporation of acetone leads to numerous air nanopores inside the polymers, which further cause strong scattering, making the DBR film opaque. Figure 3(a3) shows the measured transmission and reflection spectra of the three samples before and after the cell opening. From Fig. 3(a3), it is obvious that the three samples before the cell opening have quite high transmittance (near 80%) and reflectance (near 20%) across the whole Vis range. In contrast, after the cell opening, there is a significant decrease of the transmission and a slight decrease of the reflection, as shown in Fig. 3(b3). Moreover, when the acetone evaporated after the cell opening, air nanopores were created. Meanwhile, the formed LC nanodroplets were still left inside the polymer matrix. These air nanopores and LC nanodroplets will create a slightly larger index modulation within the film compared to the original acetone and LC nanodroplets. As a result, upon the acetone evaporation, clearly observable peaks/dips appeared on the measured reflection/transmission spectra for blue and green films. It is worth mentioning that we used different references in our spectral measurement. For transmittance measurement, we used the free-space light transmission in air as the reference, while for reflectance measurement, we used an Ag mirror as the reference. Since the Ag mirror does not have 100% reflection, the measured reflection of the DBR films will be higher than the theoretical prediction. As a result, we observed relatively high reflectance.

We have to mention that although the acetone evaporated after the LC cell was opened, the LCs were still left inside the films. To further remove the LCs trapped inside the films, we used ethanol to wash away the LCs. When the LC nanodroplets were washed away, complete air nanopores were created, resulting in a much larger index modulation. Therefore, after the removal of LCs, the nanoporous polymeric DBR films demonstrate a colored appearance. In our experiments, at three different incident angles of 7°, 14°, and 21°, we have achieved blue, green, and red-colored DBR films, respectively, as shown in Figs. 4(a1) and 4(a2), 4(b1) and 4(b2), and 4(c1) and 4(c2). We can clearly see the shiny blue, green, and red colors both macroscopically and microscopically from the samples. It is worth mentioning that a macroscopic look at DBR films shows nonuniform colors with fingerprint-like patterns, which could be mainly attributed to the nonuniform thickness of the index-matching oil in the optical contact. By accurately controlling the uniform thickness of the index-matching oil, this fingerprint-like pattern could be completely avoided, and hence a uniform color can be achieved accordingly.

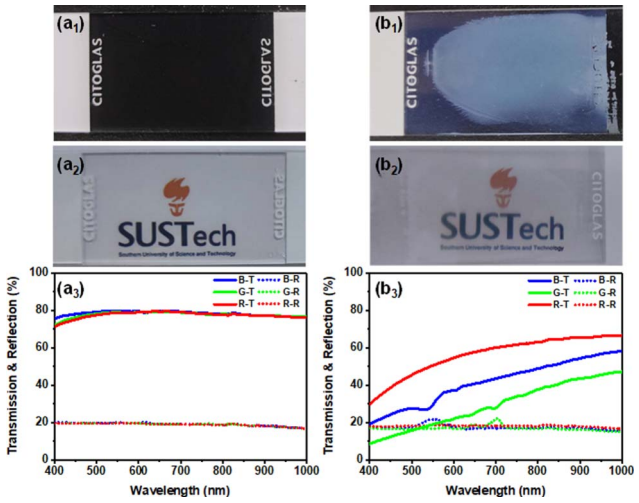


Fig. 3. Transparency-tested photos for a blue film ($a_1$), ($a_2$) before and ($b_1$), ($b_2$) after the cell opening, which were taken from the ($a_1$), ($b_1$) black and ($a_2$), ($b_2$) white backgrounds, respectively. Measured transmission and reflection spectra for blue, green, and red films ($a_3$) before and ($b_3$) after the cell opening, respectively.

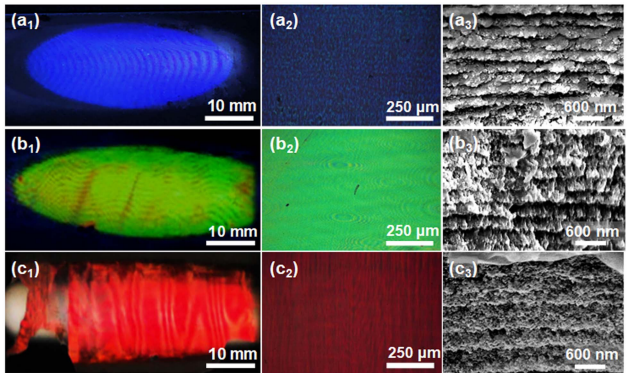


Fig. 4. ($a_1$), ($b_1$), ($c_1$) Camera photos, ($a_2$), ($b_2$), ($c_2$) optical microscopic images, and ($a_3$), ($b_3$), ($c_3$) SEM images of the ($a_1$)–($a_3$) blue, ($b_1$)–($b_3$) green, and ($c_1$)–($c_3$) red films, respectively.

To further check the morphological details of the DBR films, we have carried out the scanning electron microscopy (SEM) investigation on three colored samples. Figures 3(a3)–3(c3) show the typically observed cross-sectional SEM images that reflect the detailed morphologies of the nanoporous polymeric DBR films. It can be clearly seen that the films have a multi-layered structure that consists of alternative polymer-rich and nanopore-rich layers. Therefore, they can highly reflect a certain wavelength range of light. We can also see that as the reflection color changes from blue to red, the period of the DBR films increases gradually. The measured periods of the blue, green, and red films are ~350, ~458, and ~663 nm, respectively. A close look at the morphologies reveals that the nanopore diameters range from a few nanometers to tens of nanometers, and the porosity of the polymeric DBR structure is in a range of 20%–40%.

As mentioned, the observed Vis colors originate from the high reflection of the nanoporous DBR films. The reflection spectra of the films were therefore measured using a UV–Vis–NIR microspectrophotometer. Figure 5 shows the measured reflection spectra for the blue, green, and red samples, respectively. The red and green films have the reflection of larger than 90%, while the blue one has comparatively low reflectance but still higher than 70%. The relatively low reflection for the blue film is mainly attributed to the slightly high absorption of the polymer materials in the blue range. In addition, we can also see from Fig. 5 that the full width at half-maximum (FWHM) gradually decreases as the reflection band shifts from blue to red. The FWHMs of the reflection bands are 46, 42, and 30 nm for blue, green, and red films, respectively. The larger FWHM for the blue film might be caused by the nanopore-induced relatively stronger scattering in the blue range. As the light wavelength in the red range becomes larger, the nanopore-induced scattering becomes weak, hence resulting in a smaller FWHM.

Based on the Bragg condition, the color of the reflected film is dependent on the periodic fringe formed by the laser interference. Hence, we have theoretically calculated the

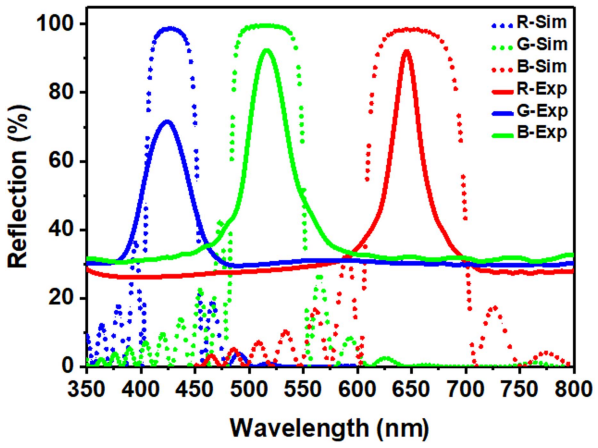


Fig. 5. Measured and simulated reflection spectra for the blue, green, and red films, respectively.

**Table 1.** The Estimated Thickness of the Polymer-Rich and Nanopore-Rich Layers for the Blue, Green, and Red Films

| Sample | Total Period (nm) | Polymer Layer Thickness (nm) | Air Layer Thickness (nm) |
|---|---|---|---|
| Blue | 350 | 204 | 146 |
| Green | 458 | 237 | 221 |
| Red | 663 | 319 | 344 |

reflection curves. The refractive indices of polymer matrices and air were assumed to be 1.47 and 1, respectively. The DBR films were all assumed to have 10 pairs of polymer-rich and nanopore-rich layers. The other data used in our calculations are tabulated in Table 1. It is worth mentioning that in our calculations, the wavelength dispersion of the refractive indices of the composed materials is not considered, because their refractive index changes in the Vis range are small enough to be ignored. We have also taken into account the shrinkage of 10%–20% of the polymerization and nanopores due to the evaporation of the solvents. It is evident that the calculated curves are in reasonable agreement with the measured ones.

In principle, the reflection band of the nanoporous polymeric DBR films is mainly determined by their filling ratio and refractive index contrast between the polymer-rich and nanopore-rich layers at the fixed period. It is quite straightforward that the reflection band will be shifted when the air nanopores are filled with other materials that have different refractive indices. Therefore, the achieved nanoporous polymeric DBRs are potentially useful for optical sensing applications. In this regard, we carried out a refractive index sensing test using our nanoporous polymeric DBRs. We have investigated the changes of the reflection spectra for the blue, green, and red films that infiltrated with four different solvents. The measured spectral changes are shown in Fig. 6. Overall, the measured reflection spectra for these three colored DBR films show a similar trend after filling with the four liquids. As the refractive index increases, the reflection peak shows an obvious redshift for each film. In addition, the reflection peak intensity decreases as well. Fig. 6(d) summarizes the peak and intensity change as functions of the refractive index. A linear change can be well observed for the blue and green films. There is slight variation for the red one, as the reflection peak becomes low and broad, causing the measurement not to be accurate enough.

Using Bragg's Law, the center wavelength of the reflection spectrum can be determined by[43]

$$\lambda_{\text{Bragg}} = 2(n_1 d_1 + n_2 d_2), \tag{1}$$

where, for our case, $n_1$ and $d_1$ are the refractive index and thickness of the polymeric layer, and $n_2$ and $d_2$ are the refractive index and thickness of the nanoporous layer. For the refractive index sensing test, the refractive index

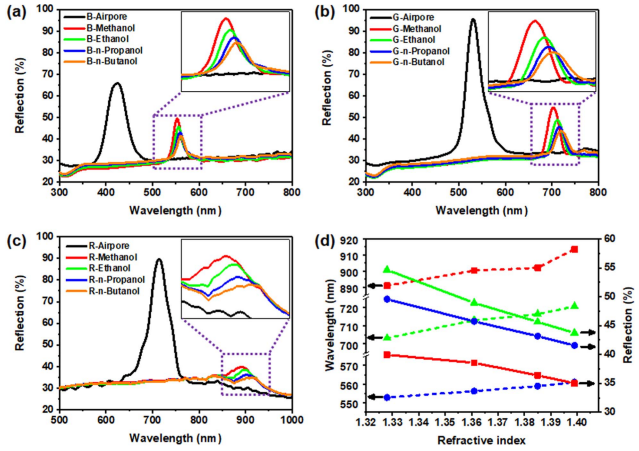


Fig. 6. Measured spectral changes of the reflection for the (a) blue, (b) green, and (c) red films that infiltrated with methanol, ethanol, *n*-propanol, and *n*-butanol, respectively. (d) Summarized peak and intensity change as the function of the refractive index.

change of the nanoporous layer (i.e., $n_2$) plays a dominant role. When $n_2$ increases, the reflected center wavelength increases as well. As a result, we observed a clear redshift of the reflection peak. On the other hand, in the extreme case, when $n_2$ increases to be equal to $n_1$ (i.e., reaching the complete index-matching condition), the DBR film will become totally transparent. There is no reflection caused by the index mismatch between the polymer-rich and nanopore-rich layers. Therefore, we also observed the intensity decrease of the reflection peak.

In summary, we have demonstrated nanoporous polymeric DBR films with periodic nanoscale porosity via a single-prism holography technique. The nanoporous DBR films consisted of alternative polymer-rich and air-nanopore-rich layers. By changing the interfering angle of two laser beams, we have achieved highly reflective nanoporous DBR films with red, green, and blue colors. Their reflectance can be larger than 70% for blue and 90% for the green and red wavelength range. We have also experimentally confirmed that the reflection band of the nanoporous DBR films can be deliberately tuned by further filling different solvents into the pores inside the films, indicating that they are highly sensitive to the refractive index. Such kinds of nanoporous polymeric DBR films could be potentially useful for many applications, such as color filters and refractive index sensors.

This work was supported in part by the National Natural Science Foundation of China (No. 61805113), Natural Science Foundation of Guangdong Province (Nos. 2017A030313034 and 2018A030310224), Shenzhen Science and Technology Innovation Commission (Nos. JCYJ20180305180635082, JCYJ20170817111349280, and GJHZ20180928155207206), Open Fund of State Key Laboratory of Applied Optics (No. SKLAO-201904), and Guangdong Innovative and Entrepreneurial Research Team Program (No. 2017ZT07C071). We acknowledge the help and discussion from Prof. Vincent Hisao at Taiwan Chi Nan University. The authors also acknowledge the assistance of SUSTech Core Research Facilities.

## References

1. P. Lova, G. Manfredi, and D. Comoretto, Adv. Opt. Mater. **6**, 1800730 (2018).
2. D. P. Puzzo, L. D. Bonifacio, J. Oreopoulos, C. M. Yip, I. Manners, and G. A. Ozin, J. Mater. Chem. **19**, 3500 (2009).
3. D. Kersey, M. A. Davis, H. J. Patrick, M. LeBlanc, K. Koo, C. Askins, M. Putnam, and E. J. Friebele, J. Lightwave Technol. **15**, 1442 (1997).
4. K.-J. Chen, H.-C. Chen, K.-A. Tsai, C.-C. Lin, H.-H. Tsai, S.-H. Chien, B.-S. Cheng, Y.-J. Hsu, M.-H. Shih, C.-H. Tsai, H.-H. Shih, and H.-C. Kuo, Adv. Funct. Mater. **22**, 5138 (2012).
5. V. Jayaraman, Z.-M. Chuang, and L. A. Coldren, IEEE J. Quantum Electron. **29**, 1824 (1993).
6. K. Neyts, P. De Visschere, D. K. Fork, and G. B. Anderson, J. Opt. Soc. Am. B **17**, 114 (2000).
7. Shelykh, M. Kaliteevskii, A. Kavokin, S. Brand, R. Abram, J. Chamberlain, and G. Malpuech, Phys. Status Solidi A **204**, 522 (2007).
8. S. Brand, M. Kaliteevski, and R. Abram, Phys. Rev. B **79**, 085416 (2009).
9. Y. J. Liu, H. T. Dai, and X. W. Sun, J. Mater. Chem. **21**, 2982 (2011).
10. Y. J. Liu, H. T. Dai, E. S. P. Leong, J. H. Teng, and X. W. Sun, Opt. Mater. Express **2**, 55 (2012).
11. V. P. Tondiglia, L. V. Natarajan, R. L. Sutherland, D. Tomlin, and T. J. Bunning, Adv. Mater. **14**, 187 (2002).
12. M. J. Escuti and G. P. Crawford, Opt. Eng. **43**, 1973 (2004).
13. Y. J. Liu and X. W. Sun, Appl. Phys. Lett. **89**, 171101 (2006).
14. Y. J. Liu and X. W. Sun, Jpn. J. Appl. Phys. **46**, 6634 (2007).
15. Z. Zheng, J. Song, Y. Liu, F. Guo, J. Ma, and L. Xuan, Liq. Cryst. **35**, 489 (2008).
16. J. Zheng, G. Sun, K. Wen, T. Wang, S. Zhuang, Y. Liu, and S. Yin, Chin. Opt. Lett. **8**, 1167 (2010).
17. G. Chen, M. Ni, H. Peng, F. Huang, Y. Liao, M. Wang, J. Zhu, V. A. L. Roy, and X. Xie, ACS Appl. Mater. Interfaces **9**, 1810 (2017).
18. Y. Zhao, X. Zhao, M.-D. Li, Z. Li, H. Peng, and X. Xie, Angew. Chem. Int. Ed. **59**, 10066 (2020).
19. W.-C. Luo, Y.-D. Xu, G.-X. Yu, S.-S. Li, H.-Y. Li, and L.-J. Chen, Opt. Express **28**, 17307 (2020).
20. T. J. Bunning, L. V. Natarajan, V. P. Tondiglia, and R. L. Sutherland, Annul. Rev. Mater. Sci. **30**, 83 (2000).
21. Y. J. Liu and X. W. Sun, Adv. Optoelectron. **2008**, 684349 (2008).
22. Y. Tomita, N. Suzuki, and K. Chikama, Opt. Lett. **30**, 839 (2005).
23. V. Pramitha, K. P. Nimmi, N. V. Subramanyan, R. Joseph, K. Sreekumar, and C. S. Kartha, Appl. Opt. **48**, 2255 (2009).
24. C. Li, L. Cao, Q. He, and G. Jin, Opt. Express **22**, 5017 (2014).
25. A. Hinojosa and S. C. Sharma, Appl. Phys. Lett. **97**, 081114 (2010).
26. M. Zhang, J. Zheng, K. Gui, K. Wang, C. Guo, X. Wei, and S. Zhuang, Appl. Opt. **52**, 7411 (2013).
27. Y. Liu, J. Zheng, T. Shen, K. Wang, and S. Zhuang, Liq. Cryst. **46**, 1852 (2019).
28. R. L. Sutherland, L. V. Natarajan, V. P. Tondiglia, and T. J. Bunning, Chem. Mater. **5**, 1533 (1993).
29. R. Caputo, L. De Sio, A. Veltri, C. Umeton, and A. V. Sukhov, Opt. Lett. **29**, 1261 (2004).
30. Y. J. Liu, X. W. Sun, J. H. Liu, H. T. Dai, and K. S. Xu, Appl. Phys. Lett. **86**, 041115 (2005).
31. Y. J. Liu, Y. B. Zheng, J. Shi, H. Huang, T. R. Walker, and T. J. Huang, Opt. Lett. **34**, 2351 (2009).

32. H. Yuan, J. Colegrove, G. Hu, T. Fiske, A. Lewis, J. Gunther, L. Silverstein, C. Bowley, G. Grawford, L. Chien, and J. Kelly, Proc. SPIE **3690**, 196 (1999).
33. L.V. Natarajan, C. K. Shepherd, D. M. Brandelik, R. L. Sutherland, S. Chandra, V. P. Tondiglia, D. Tomlin, and T. J. Bunning, Chem. Mater. **15**, 2477 (2003).
34. M. S. Park, B. K. Kim, and J. C. Kim, Polymer **44**, 1595 (2003).
35. R. Jakubiak, L. V. Natarajan, V. Tondiglia, G. S. He, P. N. Prasad, T. J. Bunning, and R. A. Vaia, Appl. Phys. Lett. **85**, 6095 (2004).
36. V. K.S. Hsiao, C. Lu, G. S. He, M. Pan, A. N. Cartwright, P. N. Prasad, R. Jakubiak, R. A. Vaia, and T. J. Bunning, Opt. Express **13**, 3787 (2005).
37. Y. J. Liu, X. W. Sun, P. Shum, H. P. Li, J. Mi, W. Ji, and X. H. Zhang, Appl. Phys. Lett. **88**, 061107 (2006).
38. Y. J. Liu, X. W. Sun, H. Elim I, and W. Ji, Appl. Phys. Lett. **90**, 011109 (2007).
39. Y. J. Liu, B. Zhang, Y. Jia, and K. S. Xu, Opt. Commun. **218**, 27 (2003).
40. R. Caputo, A. Veltri, C. P. Umeton, and A. V. Sukhov, J. Opt. Soc. Am. B **21**, 1939 (2004).
41. Y. J. Liu, X. W. Sun, H. T. Dai, J. H. Liu, and K. S. Xu, Opt. Mater. **27**, 1451 (2005).
42. V. K. S. Hsiao, T.-C. Lin, G. S. He, A. N. Cartwright, P. N. Prasad, L. V. Natarajan, V. P. Tondiglia, and T. J. Bunning, Appl. Phys. Lett. **86**, 131113 (2005).
43. V. K. S. Hsiao, K.-T. Yong, A. N. Cartwright, M. T. Swihart, P. N. Prasad, P. F. Lloyd, and T. J. Bunning, J. Mater. Chem. **19**, 3998 (2009).
44. V. K. S. Hsiao, T. J. White, A. N. Cartwright, P. N. Prasad, and C. A. Guymon, Euro. Polym. J. **46**, 937 (2010).
45. V. K. S. Hsiao, W. D. Kirkey, F. Chen, A. N. Cartwright, P. N. Prasad, and T. J. Bunning, Adv. Mater. **17**, 2211 (2005).
46. J. Shi, V. K. S. Hsiao, and T. J. Huang, Nanotechnology **18**, 465501 (2007).
47. J. Shi, V. K. S. Hsiao, T. R. Walker, and T. J. Huang, Sens. Actuators B: Chem. **129**, 391 (2008).